Building and Environment 228 (2023) 109917

Contents lists available at ScienceDirect

Building and Environment

journal homepage: www.elsevier.com/locate/buildenv

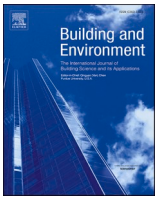

Modelling and validation of hygrothermal conditions in the air gap behind wood cladding and BIPV in the building envelope

Johannes Brozovsky *, Alessandro Nocente, Petra Rüther

Architecture, Materials and Structures, SINTEF Community, 7034, Trondheim, Norway

ARTICLE INFO

Keywords:
Hygrothermal modelling
Ventilated air cavity
Calibration
Durability
Wind barrier
Air change rate in air gap

ABSTRACT

Materials used in the building envelope are exposed to a wide range of varying and harsh conditions over extended periods. Knowledge about these precise conditions allows for improving the design of testing schemes and eventually extending the durability of building materials. In this study, a numerical model in WUFI-Pro Ver. 6.5 is calibrated with field measurements in the ventilated air gap of a Zero Emission Building located in Trondheim, Norway. Measurements were taken from September 01, 2020 until August 31, 2022 and involved recording the surface temperature of the wind barrier (19 locations) and the relative humidity of the air (11 locations) in the middle of the air gap behind wood cladding and building integrated photovoltaics. Several different air change rates in the air gap are investigated in the model. Using a constant air change rate of 100 h^{-1} showed the overall best performance ($R^2 = 0.940$ for the wind barrier's surface temperatures and $R^2 = 0.806$ for the relative humidity of air in the middle of the air gap). The largest deviations between simulation results and measurements, however, can be attributed to the uncertainty of climate data input. The developed model can be used in future studies that significantly contribute to establishing better testing schemes and test conditions for building materials such as wind barriers and adhesive tapes, and eventually improve the long-term air tightness of buildings.

1. Introduction

In energy-efficient buildings, the envelope is a key component when it comes to providing comfortable indoor spaces and reducing the energy demand for space conditioning. Furthermore, it is responsible to protect the building from damages induced by outdoor conditions such as heat, cold, wind, precipitation, and radiation. Besides the insulating properties of the building envelope, air tightness is of central importance to avoid outdoor air from entering the building which can lead to draft, higher energy demand for heating and cooling, or damage inside the envelope structures [1]. Thus, many building codes in Europe and worldwide introduced and steadily sharpened the requirements regarding the air tightness of buildings [2–5]. Air tightness or leakage is commonly measured with normalised metrics (see Table 1). They are obtained by pressurising a building and measuring the airflow necessary to keep the building at the desired pressure level. Most often, the pressure difference Δp is taken as 50 Pa and the normalised air flow is measured in air changes (ACH) per hour [h^{-1}].

There is a significant impact of air leakage through the envelope on the energy performance of a building. For Belgium and Germany it is estimated to be about 10% [6], in central and northern Spain between 10.5% and 27.4% [7], and in Poland between 16% and 28% [8]. In their numerical study, Liu et al. [9] estimated that lowering the n_{50} of Chinese multi-family homes in different cities of the hot summer and cold winter climate zone from 1 h^{-1} to 0.6 h^{-1} reduced the heating energy demand by between 4.6% and 33.5%. In an older study from 1998 by Emmerich and Persily [10], the impact of infiltration in (at that time) newer U.S. office buildings was estimated to be about 25% of the heating and 4% of the cooling load. In Australia, the potential was quantified at 1.2%–15.4% when reducing the n_{50} from 1.0 h^{-1} to 0.5 h^{-1}, depending on the local climate conditions [11]. Rode et al. [12] found that improper air-tightening and ACH about twice as high as the design value of 0.1 h^{-1} at normal pressure in an Arctic low-energy building in Sisimiut, Greenland, led to an estimated additional 20% of total heat losses through the envelope. In a parametric study by Brozovsky et al. [13], a validated building performance simulation model of a Zero Emission Building (ZEB) [14] was simulated in different cold climate locations around the world using different settings for its wind exposure. The

* Corresponding author.
E-mail address: johannes.brozovsky@sintef.no (J. Brozovsky).

https://doi.org/10.1016/j.buildenv.2022.109917
Received 28 September 2022; Received in revised form 26 November 2022; Accepted 12 December 2022
Available online 13 December 2022

Table 1
Commonly used metrics in different countries to express building air tightness (modified from Ref. [5]).

Parameter		Equation	Unit
n_x	Air change rate at x Pa	V_x/V	h^{-1}
w_x	Specific leakage rate at x Pa	V_x/A_F	$m^3\ h^{-1}\ m^{-2}$
q_x	Air permeability rate at x Pa	V_x/A_E	$m^3 h^{-1} m^{-2}$

Where:
V_x [$m^3\ h^{-1}$]: air flow rate at a pressure difference of x Pa
V [m^3]: internal volume or volume of air inside the measured building
A_F [m^2]: net floor area of the measured building
A_E [m^2]: envelope area of the measured building.

results indicated that depending on the local climate conditions of the investigated cities, the share of infiltration in total heating energy losses ranged from 2 to 3% for a wind-sheltered building, to 4–9% for an exposed building.

Generally, it was found that energy savings are larger in heating rather than cooling-dominated climates [9,15] and the results of these studies underline the importance of air tightness for energy-saving strategies in buildings. However, the average air tightness of building stocks varies greatly between different countries (see Table 2). Nevertheless, it needs to be pointed out that the reported average air tightness values from Table 2 are not directly comparable with one another as sample sizes, measurement techniques, building typologies and years of construction differed significantly between the studies.

One of the largest databases of air tightness measurements reporting the n_{50} of single-family houses exists in the USA, collected by the Lawrence Berkeley National Laboratory [5]. Several publications [16–18] analysed this database at different times and with different focuses. In general, the US building stock shows a relatively high n_{50} of overall ca. 12.0 h^{-1} compared to reported values from studies in other countries. Likewise, the 125 houses tested by Ambrose and Syme [20] in Australia, built between 2013 and 2016 show relatively high leakage with an n_{50} of on average 15.5 h^{-1}. However, Table 2 cannot be seen as a complete overview but represents only a selection of studies reporting an n_{50} value for the investigated buildings. Other noteworthy studies reporting different metrics or dwelling types than single-family houses are for instance given by Perera and Parkins [34] who report an average n_{50} of 13 h^{-1} from measurements in 385 dwellings of diverse types, ages, and wall constructions in the UK. In a more recent paper investigating the air tightness of 287 post-2006 new-build dwellings in the UK, an average q_{50} of 5.97 $m^3\ h^{-1}\ m^{-2}$ [35]. Mortensen and Bergsøe [36] found an average w_{50} of 4.3 L $s^{-1}\ m^{-2}$ and 2.9 L $s^{-1}\ m^{-2}$ for measurements in 7 renovated and 9 new single-family houses in Denmark. Paap et al. [37] tested 63 apartments in 28 multi-family houses and found a mean n_{50} of 2.3 h^{-1}. In the analysis of an extensive database of 219,000 air tightness tests of mainly residential buildings (96.3%) in France, Mélois et al. [38] identified a median air permeability rate[1] q_4 of 0.39 $m^3\ h^{-1}\ m^{-2}$ for single-family houses, and 0.57 $m^3\ h^{-1}\ m^{-2}$ for multi-family buildings. Due to the different metrics and incomplete databases regarding building volumes, envelope areas, and floor areas, it is not always possible to convert between the metrics which further impedes comparison between the studies. Poza-Casado et al. [5] present a thorough review of the main standards, metrics, and air tightness databases in Europe and North America.

In Norway, the building regulations were updated in 2017, lowering the air tightness requirements from an n_{50} of 2.5 h^{-1} for residential buildings and 1.5 h^{-1} for other buildings to 0.6 h^{-1} for all buildings [39]. Hence, the new air tightness requirements are directly in line with the Passive House standard [40]. But studies have shown that air tightness by no means remains constant over a building's service life. Measurements carried out in 52 passive houses in Germany resulted in an average n_{50} of 0.37 h^{-1}, two years later, the average value of 31 of the houses was 0.46 h^{-1}. A total of 5 buildings no longer met the requirement of <0.6 h^{-1} [41]. Similarly, Moujellad et al. [42] quantified the increase of air leakage in 61 French low-energy single-family dwellings with 18% for their mid-term sample (1–3 years after completion) and 20% for their long-term sample (3–10 years after completion).

Therefore, particular relevance falls upon the materials used for tightening buildings, such as wind barriers and tapes, as well as the solutions to avoid leakage through joints and connections between walls and windows or doors which were found to be most common [43]. To ensure long durability of tightening materials in these locations, they are usually tested with accelerated ageing methods [44–47], exposing them to a series of changing climate conditions in a laboratory setup, i.e. humidity, UV, freezing & thawing, elevated temperatures, and even mechanical stresses [47]. Most commonly, these tests involve only changing temperature and humidity conditions. Some work has been carried out on the durability of adhesive tapes, for example by Sletnes and Frank [48] who analysed durability test data from over 10 years of testing in Norway. Langmans et al. [49] tested the air tightness of wood fibre cement boards sealed with two different kinds of tapes. Their results indicated that the impact of the three artificial ageing methods on the air permeability of the tested tapes was limited. In their work, Fufa et al. [46] suggest that adhesive tapes need to maintain their sealing properties over the entire service life of the building (typically about 50–100 years, depending on the country's building code) due to their inaccessibility within the façade. This statement can be equally related to the wind barrier and other sealants in the building envelope. However, there is generally a lack of reliable tests and ageing procedures for building materials [46]. This is among others due to the uncertainty regarding the conditions a material is exposed to over a building's service life which is additionally highly dependent on the meso- and microclimate at the building's location. Especially long-term studies involving the diligent measuring and numerical modelling of these conditions are missing in the literature. This research gap was also identified by Ingebretsen et al. [50] in their review on microclimatic conditions in the air cavities of roofs and façades in Nordic climates.

Air gaps are of particular interest because ventilated constructions are the recommended and most common design to prohibit moisture-induced damage and rot in the building envelope from severe rain loads and wind-driven rain in the harsh Norwegian and Nordic climates [51,52]. Air-tightening materials are often installed directly adjacent to the air gap. Thus, knowledge about the prevailing conditions in the ventilated air gaps is needed to design adequate ageing tests [53]. To address this research gap, Riahinezhad et al. [54] carried out long-term temperature and relative humidity measurements in the 25-mm air gap behind brick cladding of a south-facing wall and below the (unventilated) roofing underlayment of a single-family building's roof facing south in Ottawa, Canada. They reported average monthly temperatures and presented a time distribution of hours within 5-degree intervals over 6 years. Furthermore, temperature and relative humidity measurements were presented for an east-facing wall over 3 years. They used their results as a basis for proposing updates to existing accelerated ageing and durability tests in laboratories.

Other research gaps identified in Ref. [50] are the investigation of long-term simulations of the microclimate in the air cavities using exterior climate data in the Nordics and validating the accuracy of humidity conditions in the air cavity using field measurements. Previous work addressing these research gaps was done in Sweden by Hägerstedt and Harderup [56]. Comparing measurements taken over almost two years in a wood frame wall with a 30 mm air gap to WUFI 5.0 simulations, the correlation was found to be worse during winter compared to the warmer seasons. However, their study did not cover the surface temperature of the wind barrier and was only done for a

[1] q_4: For a generic two-storey house with an internal volume of 320 m^3 and a loss surface area of 224 m^2, considering a flow exponent of n = 2/3, the equivalent n_{50} value of the French requirements for single-family houses (q_4 = 0.6 $m^3\ h^{-1}\ m^{-2}$) is about 2.3 h^{-1} [38].

Table 2
Comparison of reported air tightness (n50) of single-family houses in different countries.

Authors	Country	Year of construction	Type of building	Sample size [−]	Average air tightness (n_{50})
Sherman and Matson [16]	USA	1993–2000	"New houses"	8300	5.0 h^{-1}
Sherman and Dickerhoff [17]	USA	1850–1993	Single-family houses	12,902	29.7 h^{-1}
Chan et al. [18]	USA	Median = 1970[a]	Single-family detached houses	134,000	12.0 h^{-1}
Hamlin and Gusdorf [19]	Canada	1991–1996	"New conventional houses"	222	3.1 h^{-1}
		1983–1995	Houses according to R-2000 Technical Guidelines	47	1.2 h^{-1}
Ambrose and Syme [20]	Australia	2013–2016	New residential houses	125	15.5 h^{-1}
Brunsell and Uvsløkk [21]	Norway	1975–1980	Detached lightweight single-family houses	61	4.7 h^{-1}
Blom and Uvsløkk [22]	Norway	1988–2003	Terraced single-family houses	40	4.7 h^{-1}
Holøs [23]	Norway	2008	Terraced single-family houses	64	0.8 h^{-1}
Relander et al. [24]	Norway	1983–2006	Single-family lightweight houses	28	5.0 h^{-1}
Nilsson et al. [25]	Sweden	1982–1989	Detached single-family houses	44	1.3 h^{-1}
Kronvall [26]	Sweden	1976–1978	Detached single-family houses	448	3.6 h^{-1}
			Terraced single-family houses	103	3.1 h^{-1}
Kauppinen [27]	Finland	1991–1998	Single-family and detached houses	158	5.5 h^{-1}
Korpi et al. [28]	Finland	1979–2003	Timber-framed single-family houses	100	3.9 h^{-1}
Vinha et al. [29]	Finland	Younger than 10 years, measured from 2002 to 2009	Heavy-weight single-family houses	50	2.3 h^{-1}
Kalamees [30]	Estonia	1993–2004	Lightweight single-family detached houses	31	4.9 h^{-1}
Feijó-Muñoz et al. [31]	Spain	1950–after 2002	Single-family houses	18	6.1 h^{-1}
Paukštys et al. [32]	Lithuania	2016–2019	Terraced single-family houses of energy efficiency class A	>200	0.9 h^{-1}
			Terraced single-family houses of energy efficiency classes A+ and A++		0.6 h^{-1}
Solcher [33]	Germany	2014	New single-family houses	unknown	1.1 h^{-1}
			Refurbished single-family houses	unknown	1.6 h^{-1}

[a] According to the authors it is fairly representative of the whole US housing stock [18].

north-northwest facing exterior wall.

In this study, measurements in the ventilated air gap of the building envelope of a ZEB located in Trondheim, Norway, were performed over 2 years. The measurements involved recording the surface temperature of the wind barrier and the relative humidity in the middle of the air gap behind different cladding materials, i.e., wood and BIPV modules. These materials are of particular interest, as wood is the most common façade cladding material of residential buildings in Scandinavia [57] and BIPV gets more and more common in high-performance buildings in order to reach, e.g., (nearly) zero energy/emission target, passive house standard, etc. [58]. Moreover, façade and roof BIPV systems are becoming increasingly common also in Scandinavia [59,60].

The measurements taken in this study were used to calibrate a numerical model in WUFI-Pro [55] Ver. 6.5 of the building. The objective of this numerical model is to perform a parametric study in the future, simulating the investigated building with climate files, for instance, from different locations or using climate projections and help establish better testing schemes, and test conditions, and eventually improve the long-term air tightness of buildings.

In section 2 of this paper, the methodology including a description of the experimental data collection at the studied building and the settings of the numerical model are presented. Section 3 shows the simulation results and their agreement with the measurement data. Following the discussion of the results and limitations of this study in section 4, a summary of this work and suggestions for future studies are given in the conclusions in section 5.

2. Methodology

2.1. Experimental data

2.1.1. ZEB laboratory

The building that served as a test facility for the experimental data collected in this study is the ZEB Laboratory (https://zeblab.no). Completed in 2020, the ZEB Laboratory was designed and constructed to provide a research facility allowing for testing new environmentally friendly building components, solutions, strategies, and constructions as well as management processes. It serves as an arena for national and international research cooperation as well as education [61–63]. It is a 4-storey, ca. 2000 m^2 living office laboratory located in Trondheim, Norway, on the campus of the Norwegian University of Science and Technology (63°24′51″ N, 10°24′27″ E). The ambition level of the building is ZEB-COM which means that the building compensates for emissions occurring from all phases of the life cycle [64–66] through on-site renewable energy production over its assumed service life of 60 years. To achieve that, the ZEB Laboratory is equipped with thermal energy storage [67] based on phase change materials (PCM) to ensure operation at optimal efficiency for the two heat pumps. Moreover, a 181 kW_p building integrated photovoltaic (BIPV) system (see Fig. 1), on all the main façades and the pitched roof (32° inclined) produces renewable electricity of a calculated 156 MWh per year.

A special feature of the PV system is that there is also a row of PV panels on the very top of the north façade (see Fig. 1b) to harvest solar energy during the long summer days at the location's latitude when the solar azimuth is north-east in the morning and north-west in the evening. The rest of the north façade, as well as parts of the east and west façade, have a cladding of burnt wood for natural protection against weathering [68,69]. The rest of the building is either covered with BIPV or black aluminium panels.

For the building's load-bearing structure, glued laminated (glulam) timber columns, cross-laminated timber floors, stiffening internal walls, and insulated wooden framework in the external walls are used. The roof is constructed with a wood frame construction. The building envelope's U-values [W m^{-2} K^{-1}] are 0.15 (wall), 0.09 (roof), 0.10 (floor on ground) and 0.77 (windows). An air tightness test at the time of building completion showed an n_{50} of 0.3 h^{-1} [61].

2.1.2. Measurements and sensors

To meet the requirements and ambitions of a top research facility, numerous sensors are installed in the building. Most relevant for this

Fig. 1. The ZEB Laboratory viewed from the southeast (a), northeast (b), and above (c). Photos: © Nicola Lolli, 2021. Aerial photo: © Norwegian Mapping Authority.

study are the temperature and humidity sensors in the ventilated air gap of the building envelope, see for instance also [70]. While there are in total 21 temperature and 12 humidity sensor locations (see Fig. 2), not all of the sensors were used as TW3, TW4 and HW4 were not accessible for this study. Moreover, sensor TE4 has available measurement data only from October 13, 2020 13:00 CET and TN1 from March 04, 2021 10:00 CET. All sensors used in this study are covered with BIPV as external cladding material, except for the façade to the north where the cladding material is charred pine heartwood, (see Fig. 3 for wall structures). The sensors in the roof are installed at 14.3 and 22.8 m above ground and are also covered with BIPV (see Fig. 4). For this study, hourly averages of all accessible sensors per façade were made and compared to simulation results. Consequently, the measured values for, e.g., "Roof" are an arithmetic average of TR1–4 and HR2–3 at a specific hour for respectively temperature and relative humidity and so forth. The temperature measurements are publicly accessible from Ref. [71].

For this study, measurements starting September 01, 2020 until August 31, 2022 were used. The frequency of logging is every 15 min for the thermocouples and every 5 min for the relative humidity sensors. The raw data were then resampled to hourly average values to facilitate the comparison with the results from the numerical model (see section 2.1.3), for which hourly input and output data were used. These input data include two different sources of weather recordings: (1) wind speed, wind direction, air temperature, relative humidity, barometric pressure, and global horizontal radiation from the weather station on the neighbouring ZEB Test Cell Laboratory (TCL) [73] in a distance of 75 m across a parking lot (see also Fig. 1c), and (2) precipitation data from weather station *SN68860 (WMO 01257) Trondheim Voll*, operated by the Norwegian Meteorological Institute, in a distance of 2.3 km. The weather station on the ZEB TCL (1) represents the closest weather station to the study site and ensures easy and direct data access, as it is operated by the authors' research institution. Precipitation data from Trondheim's reference weather station (2) were used because they were not measured on-site during the study period. However, it is assumed that this does not lessen the accuracy of the results presented in this study. The measurement data from (2) was obtained from the Norwegian Meteorological Institute's web service *seklima* [74]. Fig. 5 shows the daily means of the most important climate variables from the weather file used for the simulations. The range of hourly recorded climate variables during the study period was −18.9 to 30.3 °C, 0.0–9.9 m s^{-1}, 2–100%, 0.0–12.6 mm, 0–729 W m^{-2}, and 0–387 W m^{-2} for air temperature, wind speed, relative humidity, precipitation, as well as direct horizontal and diffuse solar radiation, respectively. The specifications of the sensors operated by the authors' research institutions used in this work can be seen in Table 3.

Although the facility continuously collects all the data from its sensors, the records unavoidably contain a certain amount of missing data. This is due to programmed maintenance for hardware and software, as well as accidental events such as power losses. In total, 5.0% of measurements are affected (see also Fig. 5), distributed over multiple shorter periods, the longest being 10 days. These were replaced with measurements from the ZEB Living Laboratory [75] located only 280 m away from the ZEB Laboratory, where an identical weather station is mounted. However, these substitutions were only used as a placeholder and marked with a flag in the data processing. For assessing the accordance between the simulations and the measurements in the air gaps, the simulation results at the respective points in time at which this flag appears were sorted out. This is to facilitate the interpretation of results as using weather data from several different sources, particularly air temperature and solar radiation adds another dimension of error that would need to be considered. Thus, by sorting out the flagged values, systematic deviations become easier to spot in the results, and the underlying causes can be identified with less uncertainty. All in all, the comparison between simulations and measurements was done for 16, 633 out of 17,520 total data points.

2.1.3. Numerical model

The numerical calculations were carried out in WUFI-Pro Ver. 6.5 [55,76], a one-dimensional, hygrothermal simulation tool for evaluating moisture conditions in building envelopes. It is validated against EN 15026 [77]. In WUFI, the wall and roof structures were modelled (see Table 4) according to the original drawings shown in the previous

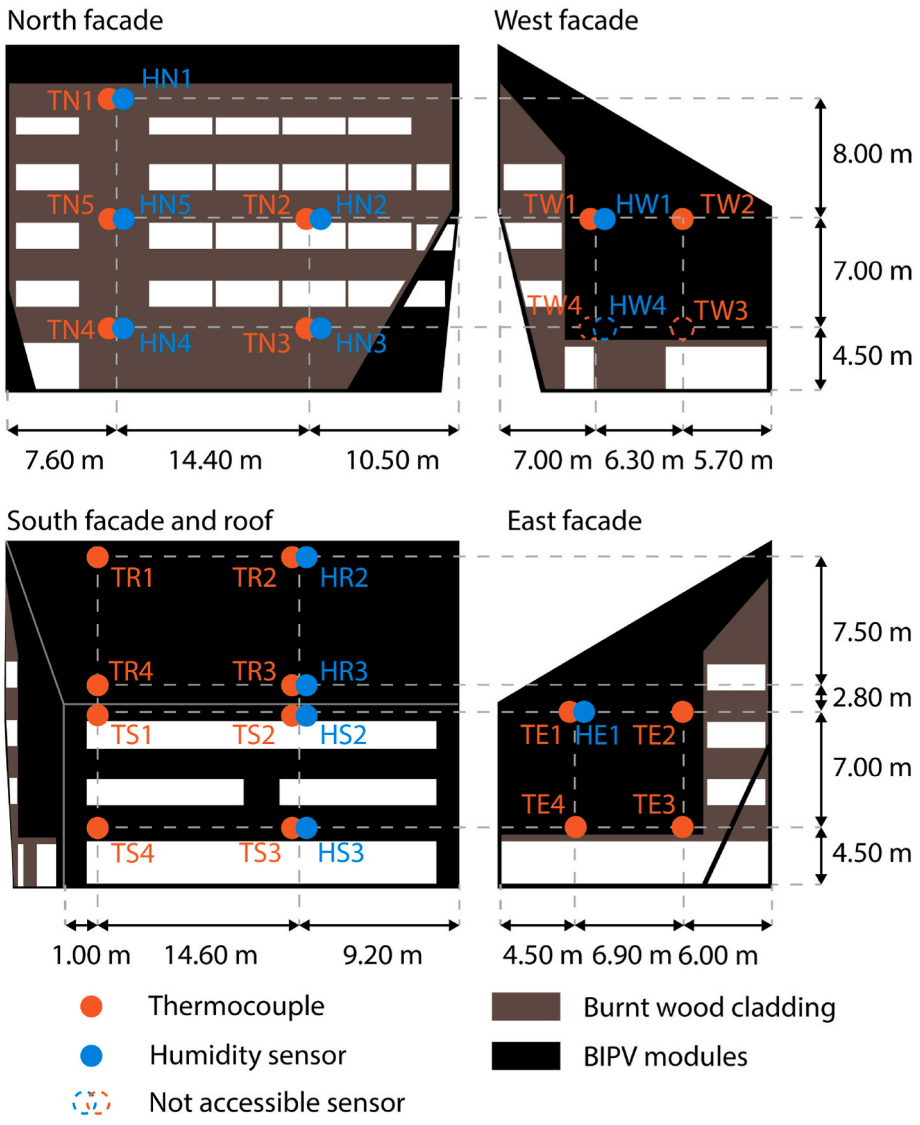

Fig. 2. Position of temperature (T, orange dots) and humidity (H, blue dots) sensors in the air gap behind the cladding on the five building envelopes north façade (N), east façade (E), south façade (S), west façade (W), and roof (R) used in this study. TW3, TW4, and HW4 were not accessible for this study. Figure not drawn to scale. (For interpretation of the references to colour in this figure legend, the reader is referred to the Web version of this article.)

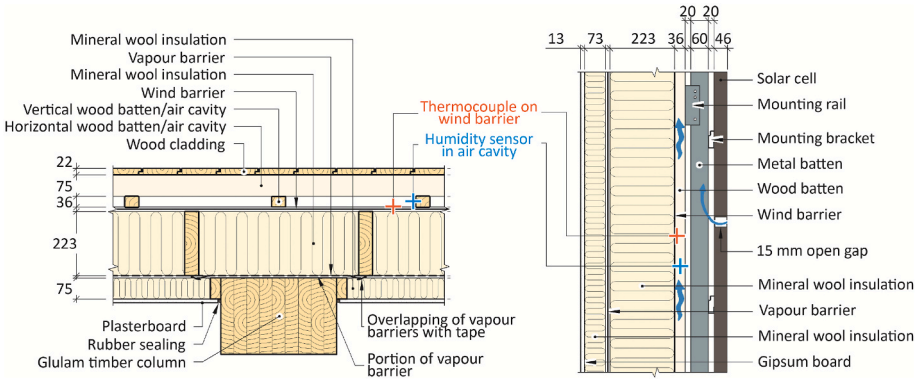

Fig. 3. Wall structures with wood cladding (left), BIPV (right), and position of thermocouple and humidity sensor in the air cavity (modified from Ref. [72]).

section. The material properties of the mineral wool, vapour barrier, wind barrier, and asphalt layer are taken from the product data sheets of the materials installed in the ZEB Laboratory. The remaining material properties are taken from the WUFI database. The data extraction locations for the result files (*monitors*) in the wall structures are according to the sensor positions in the experimental setup described earlier. For the simulations, the heat and moisture transport calculation modes together with the numerical parameters of *increased accuracy* and

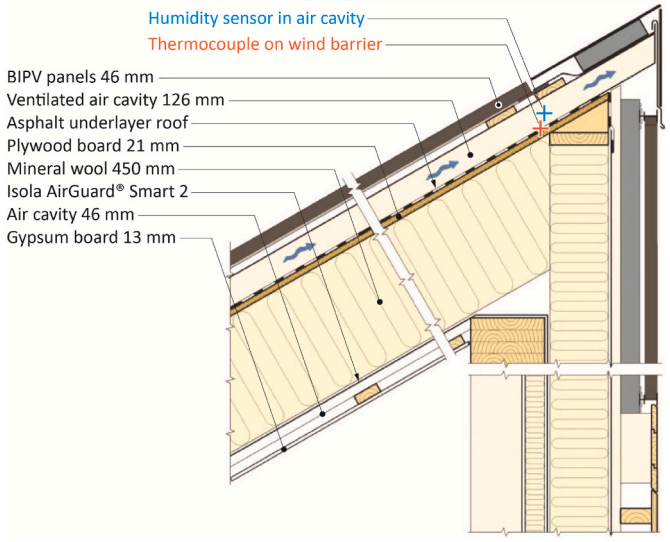

Fig. 4. Roof structure and position of thermocouple and humidity sensor in the air cavity (modified from Ref. [70]).

adapted convergence were selected in WUFI.

For the surface transfer coefficients of the external wall, WUFI's predefined values for the following parameters were selected (setting names in parentheses written in italics where applicable): 0.0588 m^2 K W^{-1} for exterior surface heat resistance (*external wall*), 0.8 for the shortwave radiation absorptivity of the wood cladding (*dark*), 0.9 for BIPV cladding (*user defined*), 0.22 for ground shortwave reflectivity (*weathered concrete*), 0.7 for adhering fraction of rain (*depending on the inclination of component*), and 0.125 m^2 K W^{-1} for the interior surface heat resistance (*external wall*). For the roof, the following settings are different from those for external walls: 0.0526 m^2 K W^{-1} for exterior surface heat resistance (*roof*), 1.0 for adhering fraction of rain (*depending on the inclination of component*). Regarding the load of wind-driven rain r_{wd} on the building envelopes, WUFI's standard procedure is used which is calculated from Eq. (1) with hourly rainfall on a horizontal surface r_h [mm h^{-1}], wind speed U_w [m s^{-1}], and model coefficients R_1 and R_2. The standard values for these coefficients were kept at $R_1 = 0$ and $R_2 = 0.1$ for vertical surfaces, and $R_1 = 1.0$ and $R_2 = 0$ for the roof.

$$r_{wd} = r_h(R_1 + R_2\ U_w) \tag{1}$$

The initial conditions in the component are set to 0.8 for relative humidity (standard value) and 6.7 °C (measured outdoor air temperature at the first time step). The indoor climate was selected as dependent on the outdoor conditions, according to EN 15026 [78]. As stated previously, the outdoor climate was composed of two sources. However, the radiation data needed to be modified before being used in the WUFI climate file. That is because the available data only comprised global horizontal radiation, though in the WUFI climate file the input of the direct and diffuse shares of solar radiation is necessary. For splitting the measured global horizontal radiation into its direct and diffuse components, the *DIRINT* (also known as *modified DISC*) model, developed by Perez et al. [79] was applied. This model showed a good performance in a worldwide validation study by Yang and Gueymard [80].

Certainly, the setting for the ACH in the air gap is an aspect of major importance for the hygrothermal behaviour of the cavity. It depends on many factors, e.g., wind velocity, wind direction, air temperature, solar radiation, material properties of the external cladding and the wall core, as well as the cavity dimensions (height and thickness), the presence of obstructions and openings, air infiltration through the external cladding, etc. [81]. Unfortunately, air velocity measurements in the air gaps of the investigated building are not available. In WUFI, there are two options regarding the ACH: (1) *constant*, and (2) *transient from a file*, i.e., a list of ACH values for every time step. Generally, literature has shown that the ACH in ventilated air gaps can have a wide range. These ranges have been reported to be between 0 and 650 h^{-1} for a 19 mm air gap [82], between 100 and 1000 h^{-1} for a 40 mm air gap [83,84] or between 230 and 310 h^{-1} for a 25 mm air gap [85]. In a study comparing different air gap depths (19, 51, 102, and 152 mm) ACHs between 30 and 1000 h^{-1} were measured. With 150 h^{-1}, the 152 mm air gap had the lowest average ACH of the investigated cases under the same meteorological conditions. The 51 mm air gap generated the highest average ACH of about 354 h^{-1} [86]. Rahiminejad and Khovalyg [81] found a general span of 100–1000 ACH, with the majority being below 600 h^{-1} in their review of numerous studies on the matter.

As a result of this uncertainty, the ACH is often set as constant in numerical studies, e.g., in Ref. [87] with 150 h^{-1}. In this study, to get the best fit between simulation results and measurements, in total nine different settings have been investigated: a constant ACH of 0, 50, 100, 150, 200, 300, 400, and 500 h^{-1}, as well as the wind speed-dependent model by Falk et al. [88] (see Eq. (2)), developed for vertically ventilated air gaps in Scandinavian conditions. However, for reasons of clarity and comprehensibility, the results are only shown for four ACH settings: a constant ACH of 50, 100, and 150 h^{-1} as well as the model by Falk et al. [88]. The other constant ACH settings showed very similar results but with slightly worse performance. The ACH setting of a constant 0 h^{-1} has been included as an extreme case.

$$ACH_{Falk} = 55.4\ U_w^{1.35} \tag{2}$$

3. Results

3.1. Field measurements

Averages of all accessible sensors per building envelope were used in this study. Consequently, the measured values for, e.g., "Roof" are an arithmetic average of TR1–4 and HR2–3 for respectively temperature and relative humidity and so forth. The measured hourly means of temperature at the surface of the wind barrier ranges from −19.6 °C up to 52.8 °C (see Fig. 6a). While the minimum temperatures are rather similar for all directions (−19.6 °C to −17.4 °C for east and the roof, respectively, all on 11.02.21 at 08:00 CET), the maximum temperatures differ more significantly, due to different intensities of solar irradiance on the individual surfaces. The highest maximum hourly averaged surface temperature of the wind barrier was recorded at the roof at 52.8 °C (03.07.21 at 13:00 CET), and the lowest maximum in the north at 33.9 °C (26.06.22 at 13:00 CET). This is largely a result of the roof's orientation towards the south and optimal inclination to maximize solar irradiation for PV production. Because the daily maximum solar irradiance occurs almost simultaneously to the daily air temperature maximum at midday on sunny days, higher temperatures can be observed in the roof's air gap than on the facades. There, due to their 90° inclination, maximum irradiance on the cladding occurs either in the morning (eastern façade) or afternoon/evening (western façade, which is also shaded), when air temperatures are lower than at midday. Even though a high solar altitude leads to less optimal incidence angle of solar radiation onto the southern façade at midday during the summer months, higher outdoor air temperatures at midday compared to the mornings lead to a higher maximum air temperature in the air gap of the southern façade (51.9 °C) than of the eastern façade (47.3 °C). A particularly low maximum temperature can be observed at the façade towards north because it receives solar radiation only in the very early morning or late evening during summer when outdoor air temperatures are usually rather low.

It is noticeable, that the median temperatures at all façades are quite similar, ranging from 7.2 °C (roof) to 7.9 °C (south). Regarding the relative humidity in the air gap, a larger variation can be seen. Across the whole building envelope, the global minimum and maximum relative humidity during the data acquisition period are respectively 8.3 and

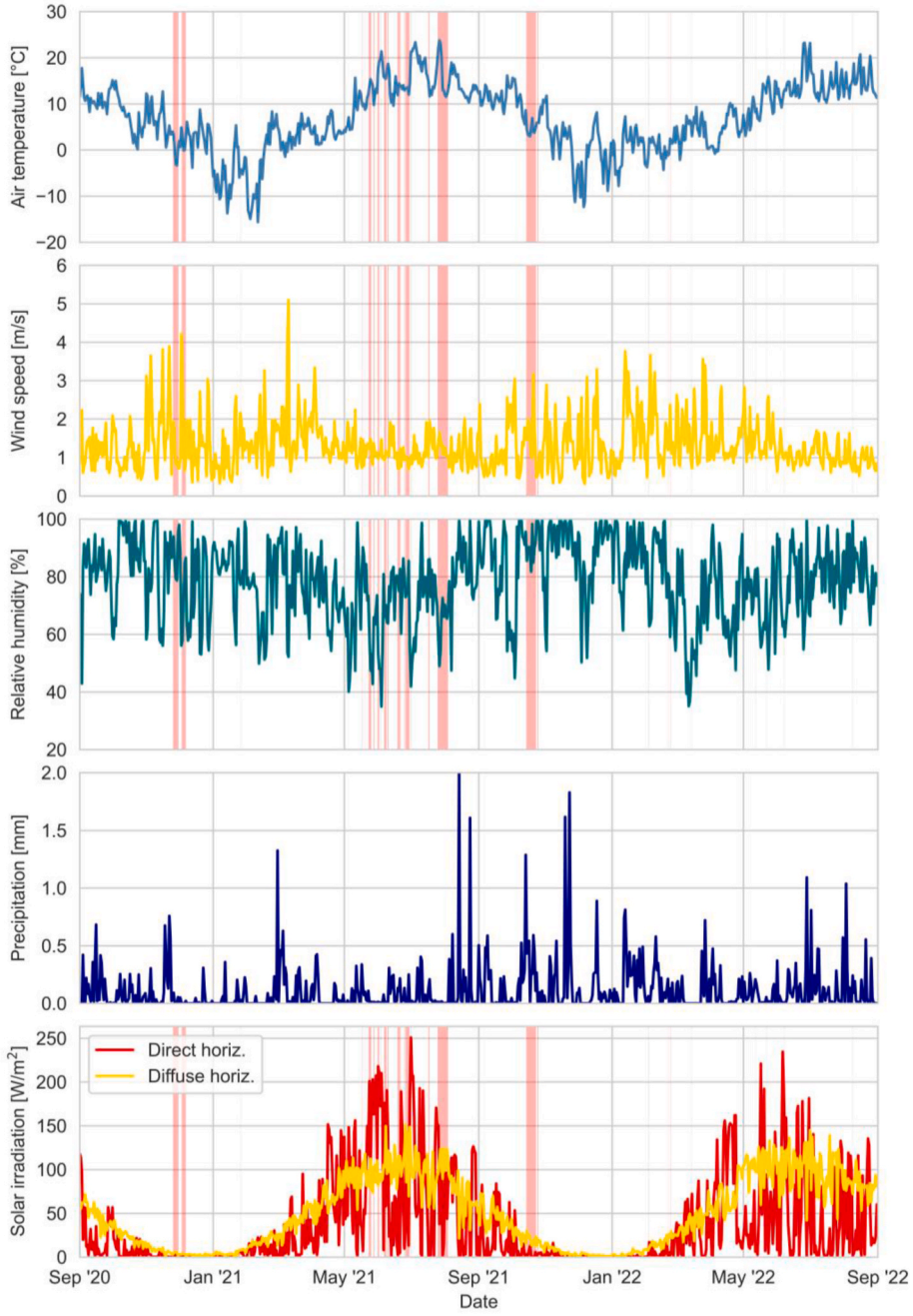

Fig. 5. Daily mean values of climate file used for the simulations with periods of data collection system malfunction at the ZEB TCL highlighted in red. (For interpretation of the references to colour in this figure legend, the reader is referred to the Web version of this article.)

99.1%, both measured in the facade to the east. There, low relative humidity measurements below 10% occur only for a short time in the early morning during late spring and early summer, when the outdoor air temperature is quite low and solar irradiation intensity on the façade is high. The median relative humidity ranges from 69.6% (south) to 75.1% (roof). Profiles of measured average hourly surface temperatures of the wind barrier and relative humidity of air in the air gaps of the different building envelopes are shown in Fig. 7.

3.2. Comparison between field measurements and simulations

In this section, the accordance between the field measurements and the WUFI simulation results is shown. The ability of the simulation model to replicate the measurements is indicated in terms of the coefficient of determination (R^2). The results are presented in Figs. 8 and 9 for the surface temperature of the wind barrier and relative humidity in the air gap, respectively. It can be seen that there is generally fair accordance between simulated and measured temperatures at the wind barrier, with an R^2 between 0.938 (ACH constant at 50 h^{-1}) and 0.940 (ACH constant at 100 h^{-1}). Regarding relative humidity in the air gap, the accordance is generally lower with an R^2 between 0.794 (ACH constant at 150 h^{-1}) and 0.807 (ACH constant at 50 h^{-1}). However, the differences are generally very small. Overall, the ACH setting of 100 h^{-1} showed the best performance, with an average R^2 of 0.873.

In the following, the performance of the simulation model with the constant ACH setting of 100 h^{-1} is presented in more detail as it showed the overall best performance (see also Table 5). Fig. 10 shows the accordance between field measurements and the WUFI results for the

Table 3
Names, measured physical quantity, measurement range and accuracy of the sensors operated by the authors' research institution used in this study.

Sensor location	Sensor type	Measured physical quantity	Measurement range	Measurement accuracy
Air gap at ZEB Lab	Thermocouple type T	Surface temperature [°C]	−40 … +85 °C	±0.5 °C
Air gap at ZEB Lab	Thin film capacity sensor	Relative humidity of air [%]	0 … 100% RH	±2% RH
Weather station at ZEB TCL	Thermocouple	Outdoor air temperature [°C]	−40 … +60 °C	±0.15 °C + 0.1 $\%_{measured}$
Weather station at ZEB TCL	Thin film capacity sensor	Outdoor relative humidity [%]	0 … 100%	±1.5% + 1.5 $\%_{measured}$
Weather station at ZEB TCL	Pyranometer	Global horizontal radiation [W m^{-2}]	0 … 2000 W m^{-2}	Class II
Weather station at ZEB TCL	Piezoresistive sensor	Outdoor barometric pressure [Pa]	600 … 1100 hPa	±50 Pa
Weather station at ZEB TCL	2-axis ultrasonic sensor	Wind speed [m s^{-1}]; wind direction [°]	0 … 60 m s^{-1}; 0 … 360°	Wind speed: ±3%; wind direction: ±2°

surface temperatures of the wind barrier and all building envelopes. The coefficient of determination R^2 varies from 0.884 on the east façade to 0.970 on the north façade. Looking at the plots of simulated over the measured relative humidity (Fig. 11), the scattering of simulation results around the measurements is generally larger than of the surface temperatures of the wind barrier. Consequently, the R^2 is lower, ranging from 0.621 on the east façade to 0.883 on the facade to the west. However, there are some clusters of data points that show a larger deviation (see for instance the highlighted areas in Fig. 10a, b, and d, as well as in Fig. 11b). The reason for these deviations will be elaborated on in the discussion in section 4.

4. Discussion

4.1. Interpretation of results

Generally, the WUFI simulation model shows satisfactory performance for the 16,633 compared data points. However, there are some envelope-specific peculiarities responsible for a major part of the deviations. At the northern façade (Fig. 10a), the WUFI simulations particularly overestimate the surface temperatures of the wind barrier when the measured temperature is between about 10 and 30 °C (see highlighted area A1 in Fig. 10a). Plotting these data points with different colours and styles according to the time and season of occurrence, showed that the largest deviations happened especially during the evenings in summer. This is when during the long Norwegian summer days, the evening sun is in the northwest and irradiates unshaded façades to the north. But due to large buildings in the northwest and west, the north façade of the investigated ZEB Laboratory is shaded extensively during these times. Consequently, the field measurements do not reflect a high incidence of solar radiation. A possible explanation for the overestimated values in area A1 in Fig. 10a is that the weather station providing the solar radiation data for the WUFI climate file is less shaded to the northwest than the ZEB Laboratory's northern façade (see also Fig. 1c).

Because of less shading of the building's northern façade but more shading of the weather station to the northeast due to large trees, the reverse effect occurs during the early morning hours mainly during the summer (see highlighted area A2 in Fig. 10a).

Similarly, an overestimation of surface temperatures of the wind barrier in the air gap behind the cladding can be observed on the western façade. In contrast to the northern façade where this occurs during the summer, the results in Fig. 10d also indicate a significant share of data points from autumn, spring, and even winter. Then, lower solar elevation angles and the large building to the west of the ZEB Laboratory cause the ZEB Laboratory's western façade to be shaded during the afternoon. Again, this effect is not reflected in the simulations, as the

Table 4
Wall and roof structures modelled in WUFI.

Component name	Layer name (from inside to outside)	Density ρ [kg m^{-3}]	Specific heat capacity c [J kg^1 K^{-1}]	Thermal conductivity λ [W m^{-1}]	Water vapour diffusion resistance factor μ [−]	Thickness [mm]
Exterior wall north (wood cladding)	Gypsum board	850	850	0.2	8.3	12.5
	Mineral wool	119	850	0.033	1.3	75
	Vapour barrier	933.33	2300	2.3	133,333	0.15
	Mineral wool	119	850	0.033	1.3	223
	Wind barrier	540	2300	2.3	20	0.5
	Ventilated air gap	1.3	1000	0.655	0.13	110
	Wood cladding	510	1600	0.13	50	22
Exterior wall east, south, and west (BIPV)	Gypsum board	850	850	0.2	8.3	12.5
	Mineral wool	119	850	0.033	1.3	73
	Vapour barrier	933.33	2300	2.3	133,333	0.15
	Mineral wool	119	850	0.033	1.3	223
	Wind barrier	540	2300	2.3	20	0.5
	Ventilated air gap	1.3	1000	0.79	0.1	130
	Aluminium (BIPV)[a]	2800	880	160	10^8	10
Roof (32° inclined towards south)	Gypsum board	850	850	0.2	8.3	12.5
	Air gap	1.3	1000	0.28	0.32	50
	Vapour barrier	460	2300	2.3	1250–64,000[b]	0.2
	Mineral wool	78	850	0.032	1.3	450
	Plywood board	500	1400	0.1	700	18
	Asphalt layer	1268	1700	0.16	100,000	4.1
	Ventilated air gap	1.3	1000	0.79	0.1	126
	Aluminium (BIPV)[a]	2800	880	160	10^8	10

[a] As it is not possible to model BIPV modules in WUFI, an aluminium panel was used instead. In accordance with the BIPV modules' exterior appearance, the colour in WUFI was set to *dark* for realistic shortwave absorption and longwave emissivity factors (0.8 and 0.9, respectively).
[b] Variable μ. Dependent on relative humidity on both sides of the vapour barrier.

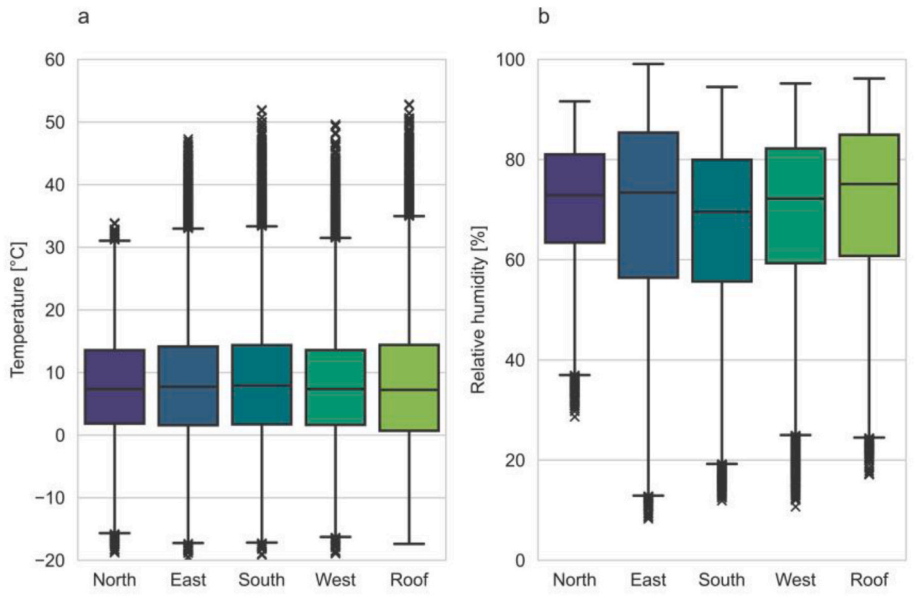

Fig. 6. Box plots of measured temperature (a) and relative humidity (b) in the air gaps of the different building envelopes at the ZEB Laboratory.

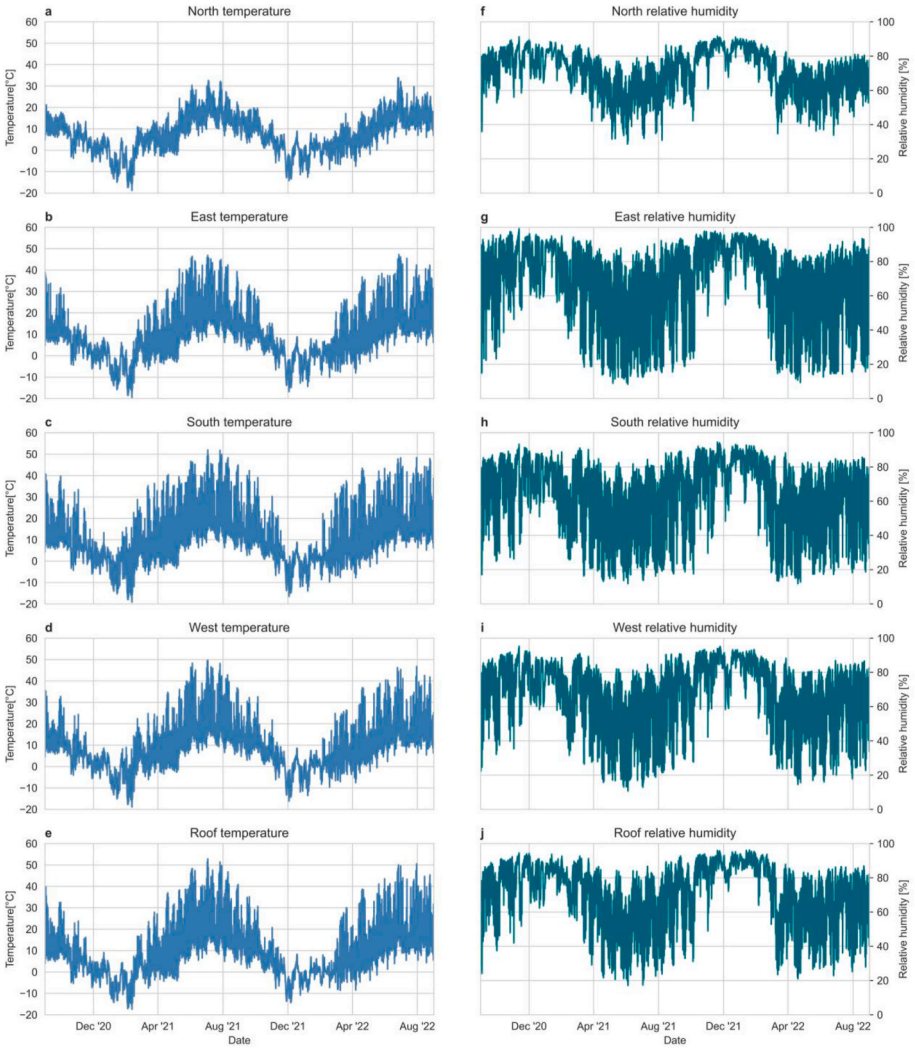

Fig. 7. Profiles of measured average hourly surface temperatures at the wind barriers (a–e) and relative humidity of air (f–j) in the air gaps of the different building envelopes over the measurement period.

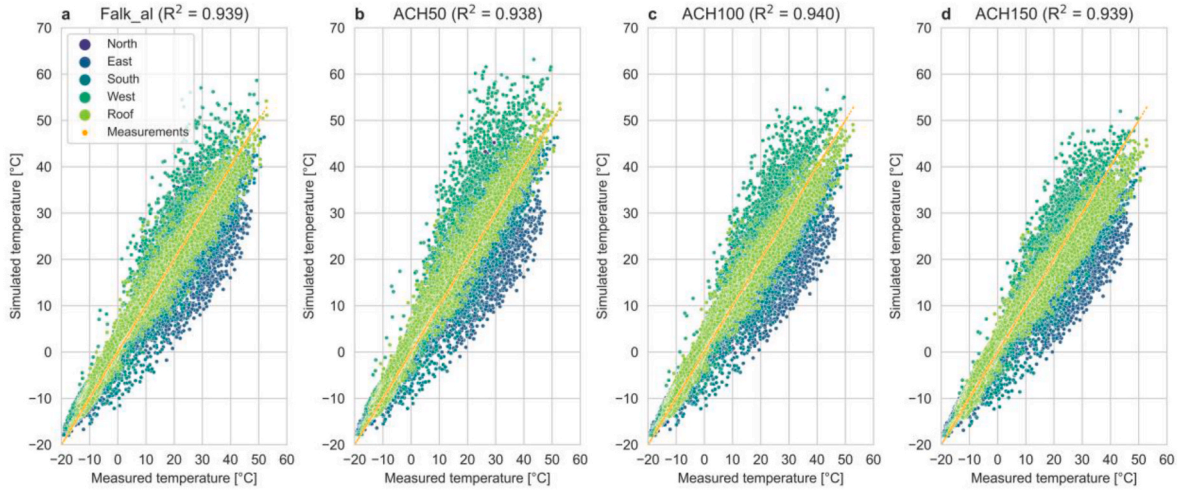

Fig. 8. Accordance between field measurements and the WUFI simulation results for the surface temperature of the wind barrier for the different ACH settings.

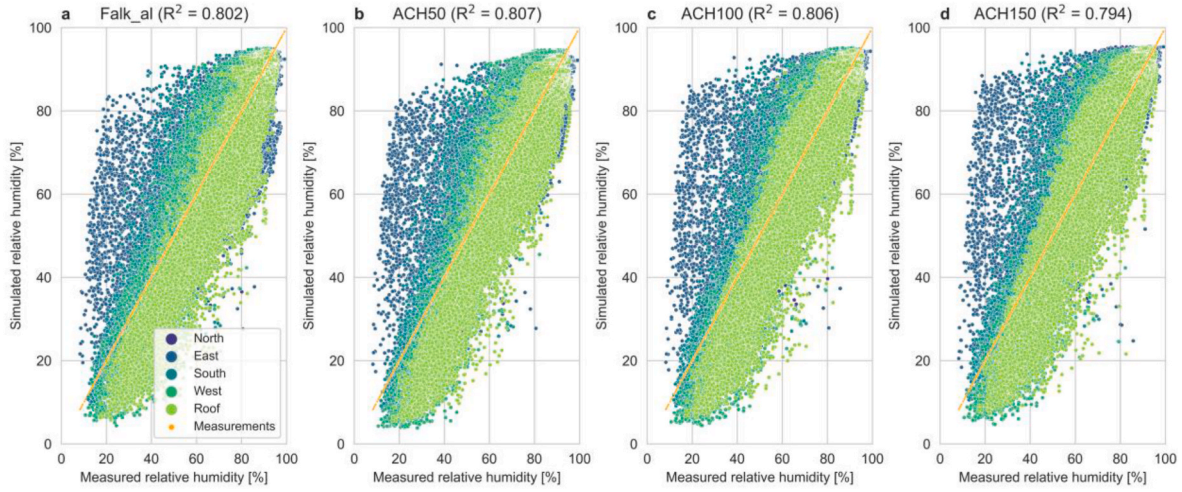

Fig. 9. Accordance between field measurements and the WUFI simulation results for the relative humidity in the air gap for the different ACH settings.

Table 5
Overview of reached accordance (R^2) between WUFI simulations and measurements with the best performance marked in bold.

ACH setting	Overall R^2 for surface temperature	Overall R^2 for relative humidity	Average R^2
Falk et al.	0.939	0.802	0.871
ACH = 0 h^{-1}	0.929	0.110	0.520
ACH = 50 h^{-1}	0.938	**0.807**	0.872
ACH = 100 h^{-1}	**0.940**	0.806	**0.873**
ACH = 150 h^{-1}	0.939	0.794	0.867
ACH = 200 h^{-1}	0.935	0.783	0.859
ACH = 300 h^{-1}	0.924	0.764	0.844
ACH = 400 h^{-1}	0.913	0.750	0.832
ACH = 500 h^{-1}	0.904	0.738	0.821

weather station on top of the TCL from which the radiation data was obtained, is significantly less shaded to the west. Therefore, WUFI calculates larger heat fluxes from solar radiation on the western façade than occur. Consequently, the simulation results overestimate the surface temperatures of the wind barrier in the air gap of the western façade, especially during the afternoon.

Again, the reverse effect was observed on the eastern façade (see the highlighted area in Fig. 10b) because of less shading of the eastern façade but more shading of the weather station to the east due to large trees. Similar to the highlighted area A2 in Fig. 10a, this effect occurred especially during the morning hours, and due to the orientation of the façade towards the east, not only in summer but also during spring, autumn, and partly even winter.

It is assumed that the discrepancy between the shading of the weather station and the actual shading of the ZEB Laboratory's façades is equally causing the deviations of the façade to the south (see Fig. 10c). Generally, it was observed that night-time data points, particularly those in winter, were best represented by the simulations, due to the absence and/or lower intensity of solar radiation. The uncertainty regarding solar radiation in the simulations is amplified by using measurements from only one horizontally mounted pyranometer and using the *DIRINT* model to split the measured global horizontal radiation into its direct and diffuse components. This error can be reduced by using one pyranometer on each of the building's facades, measuring the incoming global radiation. These have been installed at the ZEB Laboratory in the meantime. Furthermore, it is currently being worked on adding another

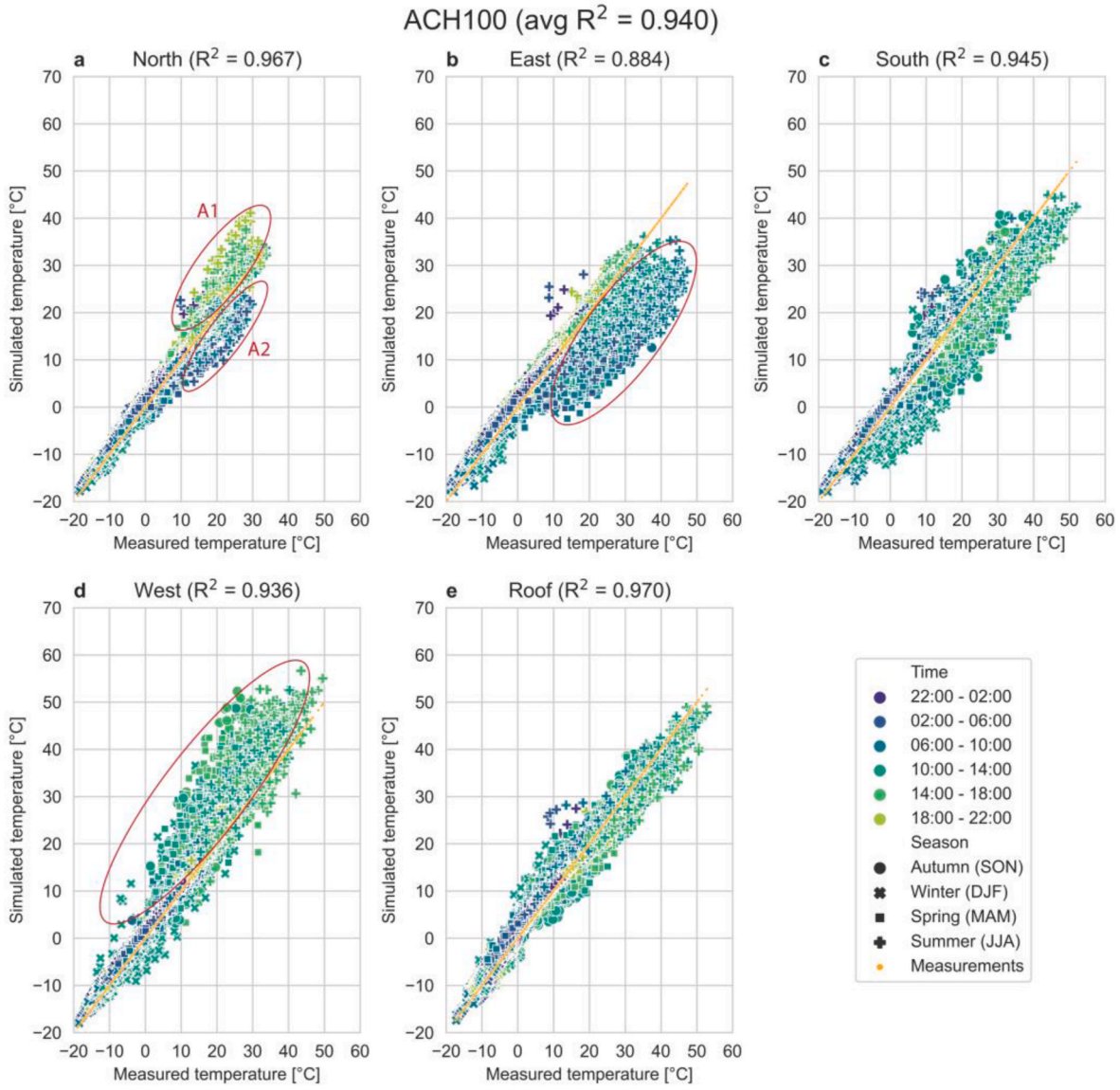

Fig. 10. Accordance between field measurements and the WUFI simulation results for the surface temperatures of the wind barrier and the different building envelopes with a constant ACH in the air gap of 100 h^{-1}.

pyranometer with a shadow ring to measure the diffuse radiation component to circumvent using a radiation-splitting model which further minimizes the error.

Regarding the simulation results for the relative humidity in the air gap behind the cladding and their accordance with the measurements, the error introduced by uncertain radiation data to the calculation of air and surface temperatures in the air gap propagates to the computation of relative humidity of the air. This is best visible in Fig. 11b (see highlighted area), as the largest deviations occur at the same points in time (in the morning) as for the simulation results for the surface temperatures of the wind barrier (see Fig. 10b).

The best-performing ACH setting for the 110-, 126-, and 130-mm air gaps in this study was a constant 100 h^{-1} in WUFI. This value is generally in line with the results reported by Girma and Tariku [86] who found that a 152 mm air gap had an average of 150 ACH in their experiments. Considering that their test wall structure did not feature any horizontal battens obstructing the vertical air flow in the air gap, a lower resulting ACH in the present study is plausible. Moreover, Kukk et al. [87] found in their sensitivity analysis that an ACH of 100 and 150 h^{-1} performed best when comparing measurements of different cross-laminated timber wall constructions to simulations. The air gap depth in their study, however, was only 28 mm.

Given these points, it becomes evident that comparing the results from studies using different designs and materials in the air gaps and are carried out in different climate conditions is nearly impossible. The extensive review of ventilation rates in ventilated air-spaces behind various wall assemblies with external cladding by Rahiminejad and Khovalyg [81] highlights the strong variability of observed ACH in ventilated air gaps. While the majority of measured values are below 400 h^{-1} across all cladding materials, the ACH in the reviewed studies ranges from 2.1 to 1461.8 h^{-1}. Again, factors that can influence the ACH in ventilated air gaps are, for instance, wind velocity, wind direction, air temperature, solar radiation, material properties of the external cladding and the wall core, as well as the cavity dimensions (height and thickness), the presence of obstructions and openings, air infiltration through the external cladding, etc. [81].

Although focusing on the hygrothermal conditions in the wall assembly behind the wind barrier, not the air gap itself, Hägerstedt and Harderup [56] reported a lower accordance between WUFI simulations and measurements during winter. In the present study, however, the

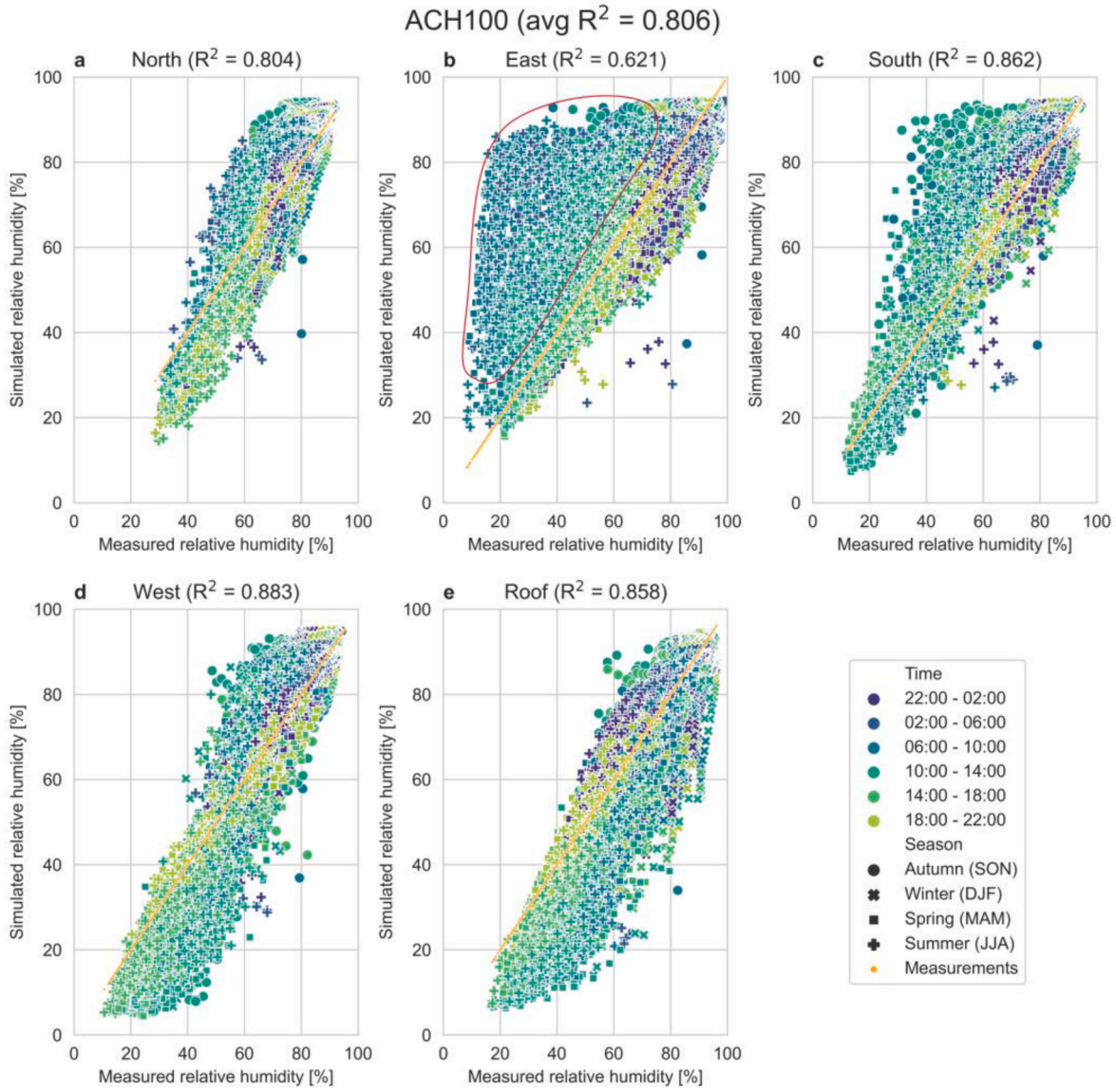

Fig. 11. Accordance between field measurements and the WUFI simulation results for relative humidity in the air gap and the different building envelopes with a constant ACH in the air gap of 100 h^{-1}.

largest deviations were found during times of increased solar irradiation as described above, i.e., especially during summer.

Regarding the investigated façade cladding materials, i.e., wood and BIPV in this study, the measurement setup did not allow for discussing the effect of the different material properties on the results. As shown in Fig. 2, measurements are only available in the ventilated air gap behind a single cladding material per envelope orientation. However, this can be part of a numerical investigation in the future, using the numerical model from this study.

4.2. Limitations

One of the main limitations of this study is related to the already mentioned uncertainty regarding the climate data input for solar radiation, i.e., (1) different shading situations for the individual façades and the weather station, and (2) using the *DIRINT* model to split global horizontal radiation into its direct and diffuse components. Furthermore, there is large uncertainty regarding the ACH in the air gap behind the cladding. While in this study all investigated cases except for one involved constant ACH settings, the ACH, in reality, is intrinsically fluctuant. Without high-quality measurements and/or validated computational fluid dynamics simulations illustrating the complex airflow patterns in the air gap behind the cladding, it is difficult to determine a relationship between external factors such as the wind conditions or solar irradiance on the building envelopes and the ACH in the air gaps for the current study. Using the wind-dependent model by Falk et al. [88] in this study also comes along with a key limitation, as it has been developed for a 2150 mm × 390 mm × 25 mm (height × width × depth) vertical air gap covered with cementitious carrier boards. In this study, this model was used equally for the air gaps in walls and the roof, as well as for different air gap depths and cladding materials (111 mm depth behind wood cladding and 136 mm depth behind BIPV cladding). Especially regarding the BIPV-covered envelopes, it is unclear how much air penetrates through the gaps between the BIPV modules which is expected to have a major effect on the ACH but was not considered in this study. Furthermore, only the wind-dependent part of the model by Falk et al. was used. However, solar radiation is also a major factor influencing the ACH in an air gap. As the *de facto* incoming solar radiation on each building envelope is unknown due to the complex shading situation resulting from the surrounding buildings and hilly

terrain, a relation between solar radiation and ACH in the air gap was not included in the model. Moreover, the simplified representation of the BIPV modules in WUFI is a limitation of the model. In this study, a 10 mm aluminium panel was used and the electrical properties and components of BIPV were omitted.

Further limitations that introduce uncertainties in the model originated in the fact that WUFI-Pro is a one-dimensional simulation tool while the real processes in the air gap are three-dimensional. In addition, precipitation data was not available at the studied building's immediate location, thus recordings from a weather station at a 2.3 km distance were used. Related to that, also the load of wind-driven rain on the vertical building envelopes is unknown and WUFI's standard procedure for its calculation was applied. Equally, it is unknown how much rain penetrates through the gaps between the BIPV modules into the air gap. Another limitation comes from the measurement location of conditions in the air gap at 11.5 m height above ground. This cannot be entered as a parameter in the software. Further on, a constant surface heat transfer coefficient for both the convective and radiative parts was used, while they are both transient. Another challenge was related to the gaps in the recordings of the weather data. Although these gaps were filled with weather data from close by, flagged, and sorted out for the results shown in this article, a small "upstart error" is introduced in the first few time steps after each gap. This is because they respond to the uncertain weather conditions used to fill in the gaps and due to their storage capacity regarding thermal energy and moisture that prolong this response beyond the actual gaps.

Considering these limitations, it needs to be highlighted that the results from this paper might only be transferred to other wall structure designs and orientations after careful consideration of the similarities and differences involved.

5. Conclusions

In this study, measurements in the ventilated air gap of the building envelope of a Zero Emission Building located in Trondheim, Norway, were performed for 2 full years, starting September 01, 2020 until August 31, 2022. They involved recording the surface temperature of the wind barrier and the relative humidity of the air in the middle of the air gap behind wood and BIPV cladding. These measurements were used to calibrate a numerical model in WUFI-Pro Ver. 6.5. Due to the uncertainty regarding the air change rate (ACH) in the air gap, several different settings have been investigated. Taking the average R^2 of the wind barrier's surface temperature and the relative humidity of the air in the middle of the air gap as a basis, the setting using a constant ACH of 100 h^{-1} showed overall the best performance with an average R^2 of 0.873 ($R^2 = 0.940$ for the wind barrier's surface temperature and $R^2 = 0.806$ for the relative humidity of air in the middle of the air gap). The differences in terms of average R^2 between the different ACH settings in WUFI, however, are minor (average R^2 of 0.872, 0.866 and 0.870 for an ACH of 50 h^{-1}, 150 h^{-1} and according to Falk et al. [88]). The largest deviations between simulation results and measurements, can be attributed to the uncertainty of climate data input regarding solar radiation. During the night, and especially during the winter when the days are short and the intensity of solar irradiance is low, the simulation results strongly agreed with field measurements. During the daytime, on the other hand, the different shading situations of the individual building envelopes and the weather station providing the data for the simulation's climate input caused major deviations of up to several tens of degrees Celsius and per cent relative humidity. But overall, the developed WUFI model showed a convincing performance.

The developed WUFI model can be used to predict the conditions inside the air gap of buildings with comparable wall structures and materials in similar climatic conditions. Those could also involve climate projections or weather extremes. Before applying the model in different climates that come along with particularly hot summer conditions and extended periods of intense solar irradiation, the model should be tested using more precise recordings of solar radiation. Further studies could be also done on the ACH in the air gaps, by installing anemometers and correlating the recorded air flow to for instance local wind conditions or solar irradiance on the façades.

It is expected that this work can significantly contribute to establishing better testing schemes and test conditions for air-tightening materials such as wind barriers and adhesive tapes, and eventually improve the long-term air tightness of buildings.

CRediT authorship contribution statement

Johannes Brozovsky: Visualization, Validation, Software, Project administration, Methodology, Investigation, Formal analysis, Writing – original draft, Writing – review & editing. **Alessandro Nocente:** Writing – review & editing, Validation, Resources, Methodology, Data curation. **Petra Rüther:** Writing – review & editing, Supervision, Methodology, Conceptualization.

Declaration of competing interest

The authors declare that they have no known competing financial interests or personal relationships that could have appeared to influence the work reported in this paper.

Data availability

The data used in this research will be made available for the public at a later point in time in 2023.

Acknowledgements

The authors gratefully acknowledge the financial support by the Research Council of Norway and several partners through the *TightEN* project [grant number 294894], the Centre of Research-based Innovation *Klima 2050* (www.klima2050.no) [grant number 237859], and the ZEB Laboratory project [grant number 245663]. The authors also thank Odne Oksavik for providing and processing part of the measurement data used in this study, as well as Tore Kvande for his valuable input and support.

References

[1] C. Younes, C.A. Shdid, G. Bitsuamlak, Air infiltration through building envelopes: a review, J. Build. Phys. 35 (3) (2012) 267–302, https://doi.org/10.1177/1744259111423085.

[2] V. Leprince, F.R. Carrié, M. Kapsalaki, Building and ductwork airtightness requirements in Europe - comparison of 10 European countries, 13-14 September, in: Proceedings from the 38th AIVC/6th Tightvent/4th Venticool Conference in Nottingham, UK, 2017, 192–201.

[3] S.J. Emmerich, A.K.U.S. Persily, Commercial building airtightness requirements and measurements, 12-13 October, in: Proceedings from the 32nd AIVC and 1st Tightvent Conference in Brussels, Belgium, 2011, 134–7.

[4] M.J. Limb, A Review of International Ventilation, Airtightness, Thermal Insulation and Indoor Air Quality Criteria. Coventry (UK), 2001.

[5] I. Poza-Casado, V.E. Cardoso, R.M. Almeida, A. Meiss, N.M. Ramos, M.Á. Padilla-Marcos, Residential buildings airtightness frameworks: a review on the main databases and setups in Europe and North America, Build. Environ. 183 (2020), 107221, https://doi.org/10.1016/j.buildenv.2020.107221.

[6] F.R. Carrié, B. Rosenthal, An Overview of National Trends in Envelope and Ductwork Airtightness, 29, 2008. AIVC Ventilation Information Paper.

[7] A. Meiss, J. Feijó-Muñoz, The energy impact of infiltration: a study on buildings located in north central Spain, Energy Effic. 8 (1) (2015) 51–64, https://doi.org/10.1007/s12053-014-9270-x.

[8] A. Miszczuk, Influence of air tightness of the building on its energy-efficiency in single-family buildings in Poland, in: MATEC Web Conf, vol. 117, 2017, https://doi.org/10.1051/matecconf/201711700120.

[9] Y. Liu, B. Li, X. Cao, The research on the influence of building air tightness to energy consumption of residential building in a hot summer and cold winter zone in China, in: IOP Conf. Ser.: Mater. Sci. Eng, vol. 609, 2019, 72003, https://doi.org/10.1088/1757-899X/609/7/072003, 7.

[10] S.J. Emmerich, A.K. Persily, Energy impacts of infiltration and ventilation in U.S. Office buildings using multizone airflow simulation, in: Proceedings of IAQ and Energy 98 Conf. In New Orleans, LA, 1998, pp. 191–203, 22-27 Oct.

[11] A.M. Egan, Air tightness of Australian office buildings: reality versus typical assumptions used in energy performance simulation, in: Proc. 12th Int. Build. Perform. Simul. Assoc. Conf. (Sydney, Australia), 2011, pp. 32–39. Proceedings of the 12th IBPSA Conference, Sydney, Australia, November 14-26.

[12] C. Rode, P. Vladyková, M. Kotol, Air tightness and energy performance of an arctic low-energy house, in: Proceedings of the 5th International Symposium on Building and Ductwork Air-Tightness, 2010.

[13] J. Brozovsky, N. Gaitani, A. Gustavsen, Characterisation of heat losses in zero emission buildings (ZEB) in cold climate, in: Proc. 16th Int. Build. Perform. Simul. Assoc. Conf. (Rome, Italy), 2019, pp. 343–350, https://doi.org/10.26868/25222708.2019.210560.

[14] A.G. Hestnes, N.L. Eik-Nes (Eds.), Zero Emission Buildings. Bergen (Norway), Fagbokforlaget, 2017.

[15] S.J. Emmerich, T.P. McDowell, W. Anis, Simulation of the impact of commercial building envelope airtightness on building energy utilization, Build. Eng. 113 (2007) 379–399.

[16] M.H. Sherman, N.E. Matson, Air Tightness of New U.S. Houses: A Preliminary Report. Berkeley, 2002.

[17] M.H. Sherman, D. Dickerhoff, Air-tightness of U.S. Dwellings, Build. Eng. 104 (2) (1998) 1359–1367.

[18] W.R. Chan, J. Joh, M.H. Sherman, Analysis of air leakage measurements of US houses, Energy Build. 66 (2013) 616–625, https://doi.org/10.1016/j.enbuild.2013.07.047.

[19] T. Hamlin, J. Gusdorf, Airtightness and Energy Efficiency of New Conventional and R-2000 Housing in Canada, 1997. Ottawa, Ontario, 1997.

[20] M. Ambrose, M. Syme, Air tightness of new Australian residential buildings, Proc Eng 180 (2017) 33–40, https://doi.org/10.1016/j.proeng.2017.04.162.

[21] J. Brunsell, S. Uvsløkk, Air Tightness in Dwellings - Results from Air Tightness Measurements in Newer Norwegian Dwellings, 1980 [in Norwegian].

[22] P. Blom, S. Uvsløkk, Build Tight!, 2012 [in Norwegian].

[23] S. Holøs, Lekkasjemodell for Småhusboliger, 2010 [Leakage model for terraced houses].

[24] T.-O. Relander, J.V. Thue, T. Aurlien, T. Kvande, B. Time, Airtightness and air leakages of Norwegian wood-frame houses, in: Proceedings from the 4th International Building Physics Conference, 15-18 June 2009, Istanbul, Turkey, 2009.

[25] I. Nilsson, L. Rosell, E. Thorstensen, Air Quality and Ventilation in Airtight Houses - Follow up of 44 Houses during the Years 1982–89, 1993 [in Swedish].

[26] J. Kronvall, Airtightness: Measurements and Measurement Methods. Stockholm, Sweden, 1980.

[27] T. Kauppinen, Air tightness of buildings in Finland, in: Proceedings of SPIE 4360, Thermosense XXIII, March 23 2001.

[28] M. Korpi, J. Vinha, J. Kurnitski, Airtightness of timber-framed houses with different structural solutions, in: Proceedings of IX International Conference on Performance of Exterior Envelopes of Whole Buildings, 5-10 December, Session XIB, (CD), Florida, USA, 2004.

[29] J. Vinha, E. Manelius, M. Korpi, K. Salminen, J. Kurnitski, M. Kiviste, et al., Airtightness of residential buildings in Finland, Build. Environ. 93 (2015) 128–140, https://doi.org/10.1016/j.buildenv.2015.06.011.

[30] T. Kalamees, Air tightness and air leakages of new lightweight single-family detached houses in Estonia, Build. Environ. 42 (6) (2007) 2369–2377, https://doi.org/10.1016/j.buildenv.2006.06.001.

[31] J. Feijó-Muñoz, R.A. González-Lezcano, I. Poza-Casado, M.Á. Padilla-Marcos, A. Meiss, Airtightness of residential buildings in the Continental area of Spain, Build. Environ. 148 (2019) 299–308, https://doi.org/10.1016/j.buildenv.2018.11.010.

[32] V. Paukštys, G. Cinelis, J. Mockienė, M. Daukšys, Airtightness and heat energy loss of mid-size terraced houses built of different construction materials, Energies 14 (19) (2021) 6367, https://doi.org/10.3390/en14196367.

[33] O. Solcher, Building airtightness in Germany - what are the driving forces?, 23-24 September, in: Proceedings from the 36th AIVC/5th Tightvent/3rd Venticool Conference in Madrid, Spain, 2015, 21.

[34] E. Perera, L. Parkins, Airtightness of UK buildings: status and future possibilities, Environ. Policy Pract. 2 (2) (1992) 143–160.

[35] W. Pan, Relationships between air-tightness and its influencing factors of post-2006 new-build dwellings in the UK, Build. Environ. 45 (11) (2010) 2387–2399.

[36] L.H. Mortensen, N.C. Bergsøe, Air tightness measurements in older Danish single-family houses, Energy Proc. 132 (2017) 825–830, https://doi.org/10.1016/j.egypro.2017.10.016.

[37] L. Paap, A. Mikola, T.-A. Kõiv, T. Kalamees, Airtightness and ventilation of new Estonian apartments constructed 2001-2010, 10-11 October, in: Proceedings from the 33rd AIVC and 2nd Tightvent Conference in Copenhagen, Denmark, 2012, 177–80.

[38] A.B. Mélois, B. Moujalled, G. Guyot, V. Leprince, Improving building envelope knowledge from analysis of 219,000 certified on-site air leakage measurements in France, Build. Environ. 159 (2019), 106145, https://doi.org/10.1016/j.buildenv.2019.05.023.

[39] Norwegian Building Authority, Regulations on Technical Requirements for Construction Works, 2017.

[40] Passiv House Institute, Criteria for the Passive House, EnerPHIt and PHI Low Energy Building Standard. Darmstadt, Germany, 2022.

[41] H. Erhorn-Kluttig, H. Erhorn, H. Lahmidi, Airtightness Requirements for High Performance Building Envelopes, 2009.

[42] B. Moujellad, S. Berthault, A. Litvak, V. Leprince, D. Louet, G. Frances, et al., Onsite evaluation of building airtightness durability: long-term and mid-term field measurements study of 61 French low energy single family dwellings, 15-16 October, in: Proceedings from the 40th AIVC/8th Tightvent/6th Venticool Conference in Ghent, Belgium, 2019, 776–87.

[43] L. Gullbrekken, N. Schjøth Bunkholt, S. Geving, P. Rüther, Air leakage paths in buildings: typical locations and implications for the air change rate, E3S Web Conf. 172 (2020) 5010, https://doi.org/10.1051/e3sconf/202017205010.

[44] P. Ylmén, M. Hansén, J. Romild, Durability of air tightness solutions for buildings, 24-25 September, in: Proceedings from the 35th AIVC/4th Tightvent/2nd Venticool Conference in Poznan, Poland, 2014, 268–78.

[45] A. Litvak, F. Allègre, B. Moujalled, V. Leprince, Assessment of the durability of airtightness products in laboratory controlled conditions: development and presentation of the experimental protocol, in: Proceedings from the 40th AIVC/8th Tightvent/6th Venticool Conference in Ghent, Belgium, 2019, pp. 788–800, 15-16 October.

[46] S.M. Fufa, N. Labonnote, S. Frank, P. Rüther, B.P. Jelle, Durability evaluation of adhesive tapes for building applications, Construct. Build. Mater. 161 (2018) 528–538.

[47] T. Ackermann, Alternating loads - a method for testing the durability of adhesives in air tightness layers, 28-29 March, in: Proceedings of the AIVC-TightVent International Workshop in Brussels, Belgium, 2012, 61–6.

[48] M. Sletnes, S. Frank, Performance and durability of adhesive Tapes for building applications. From product documentation to scientific knowledge (and back again), in: XV International Conference on Durability of Building Materials and Components. eBook of Proceedings, CIMNE, 2020.

[49] J. Langmans, T.Z. Desta, L. Alderweireldt, S. Roels, Durability of self-adhesive tapes for exterior air barrier applications: a laboratory investigation, Int. J. Vent. 16 (1) (2017) 30–41, https://doi.org/10.1080/14733315.2016.1252154.

[50] S.B. Ingebretsen, E. Andenæs, T. Kvande, Microclimate of air cavities in ventilated roof and façade systems in nordic climates, Buildings 12 (5) (2022) 683, https://doi.org/10.3390/buildings12050683.

[51] N.S. Bunkholt, B. Time, T. Kvande, Ventilated Claddings: Recommendations for Climate Adjustment, 2021 [In Norwegian].

[52] SINTEF Building and Infrastructure, 542.003 Two-stage sealing against driving rain on facades. Ventilated cladding and joints [In Norwegian]. [November 09, Available from: https://www.byggforsk.no/dokument/470/totrinnstetning_mot_slagregn_paa_fasader_luftede_kledninger_og_fuger#i12, 2022.

[53] P. Rüther, K. Gradeci, M. Sletnes, Predominant climate exposure strains - thermal degradation testing compared to historical and future climate scenarios, in: XV International Conference on Durability of Building Materials and Components. eBook of Proceedings, CIMNE, 2020.

[54] M. Riahinezhad, A. Eve, M. Armstrong, P. Collins, J.-F. Masson, Field temperature and moisture loads from a building envelope as the basis for accelerated aging of barrier membranes, Can. J. Civ. Eng. 46 (44) (2019) 969–978.

[55] Fraunhofer Institute for building physics IBP. WUFI, July 28, Available from: https://wufi.de/en/software/wufi-pro/, 2022.

[56] S.O. Hägerstedt, L.-E. Harderup, Comparison of measured and calculated temperature and relative humidity with varied air flow, in: Proceedings of the 9th Nordic Symposium on Building Physics - NSB 2011, vol. 1, 2011, pp. 147–154.

[57] K. Nore, Hygrothermal Performance of Ventilated Wooden Cladding, Norwegian University of Science and Technology (NTNU), Trondheim, Norway, 2010.

[58] A. Kylili, P.A. Fokaides, Investigation of building integrated photovoltaics potential in achieving the zero energy building target, Indoor Built Environ. 23 (1) (2014) 92–106, https://doi.org/10.1177/1420326X13509392.

[59] M. Formolli, G. Lobaccaro, J. Kanters, Solar energy in the nordic built environment: challenges, opportunities and barriers, Energies 14 (24) (2021) 8410, https://doi.org/10.3390/en14248410.

[60] M. Devetaković, D. Djordjević, M. Radojević, A. Krstić-Furundžić, B.-G. Burduhos, G. Martinopoulos, et al., Photovoltaics on landmark buildings with distinctive geometries, Appl. Sci. 10 (19) (2020) 6696, https://doi.org/10.3390/app10196696.

[61] A. Nocente, B. Time, H.M. Mathisen, T. Kvande, A. Gustavsen, The ZEB Laboratory: the development of a research tool for future climate adapted zero emission buildings, J. Phys.: Conf. Ser. 2069 (1) (2021), 12109, https://doi.org/10.1088/1742-6596/2069/1/012109.

[62] B. Time, A. Engebø, M. Christensen, O. Dalby, T. Kvande, The design process for achievement of an office living laboratory with a ZEB standard, in: IOP Conf. Ser.: Earth Environ. Sci, vol. 352, 2019, 12053, https://doi.org/10.1088/1755-1315/352/1/012053, 1.

[63] B. Time, H.M. Mathisen, A. Førland-Larsen, A. Ramberg Myhr, T. Jacobsen, A. Gustavsen, ZEB laboratory - research possibilities, SINTEF Notes 33 (2019).

[64] ISO 14040:2006, Environmental Management - Life Cycle Assessment - Principles and framework;13.020.10; 13.020.60, International Organization for Standardization, Geneva, Switzerland, 2006.

[65] ISO 14044:2006, Environmental Management - Life Cycle Assessment - Requirements and guidelines;13.020.60; 13.020.10, International Organization for Standardization, Geneva, Switzerland, 2006.

[66] EN 15978:2011, Sustainability of Construction Works - Assessment of Environmental Performance of Buildings - Calculation method;91.040.99, European Committee for Standardization, Brussels, Belgium, 2011.

[67] A. Sevault, F. Bøhmer, E. Næss, L. Wang, Latent heat storage for centralized heating system in a ZEB living laboratory: integration and design, IOP Conf. Ser.: Earth Environ. Sci. vol. 352 (1) (2019), 12042, https://doi.org/10.1088/1755-1315/352/1/012042.

[68] D. Ebner, R. Stelzer, M.C. Barbu, Study of wooden surface carbonization using the traditional Japanese yakisugi technique, Pro Ligno 15 (4) (2019) 278–283.

[69] D. Machová, A. Oberle, L. Zárybnická, J. Dohnal, V. Šeda, J. Dömény, et al., Surface characteristics of one-sided charred beech wood, Polymers 13 (10) (2021), https://doi.org/10.3390/polym13101551.
[70] N.S. Bunkholt, L. Gullbrekken, B. Time, T. Kvande, Pitched unventilated wood frame roof with smart vapour barrier – field measurements, J. Phys.: Conf. Ser. 2069 (1) (2021), 12007, https://doi.org/10.1088/1742-6596/2069/1/012007.
[71] P. Rüther, O. Oksavik, TightEN - ZEB-Laboratory - Temperature behind cladding, November 22, Available from: https://doi.org/10.5281/zenodo.7042548, 2022.
[72] L. Svenning, R. Moschetti, T. Kvande, L. Gullbrekken, B. Time, Airtightness development in large timber buildings: case study of a zero emission building in Norway, 5th-7th September, in: Proceedings of the 5th Central European Symposium on Building Physics, 2022. Bratislava, Slovakia (in press).
[73] F. Goia, C. Schlemminger, A. Gustavsen, The ZEB Test Cell Laboratory. A facility for characterization of building envelope systems under real outdoor conditions, Energy Proc. 132 (2017) 531–536, https://doi.org/10.1016/j.egypro.2017.09.718.
[74] Norwegian Centre for Climate Services, seKlima: observations and weather statistics, July 25, Normals (2022). Available from: https://seklima.met.no.
[75] F. Goia, L. Finocchiaro, A. Gustavsen, The ZEB Living Laboratory at the Norwegian University of Science and Technology: a zero emission house for engineering and social science experiments, in: 7th Passivhus Norden - Conference Proceedings, 2015.
[76] Fraunhofer Institute for Building Physics IBP, WUFI Pro 6 Manual, 2019.
[77] Fraunhofer Institute for Building Physics IBP, WUFI Passes Benchmark Test of EN 15026: WUFI Complies with the General Requirements of Standard EN 15026 and Passes its Benchmark Test, 2007.
[78] EN 15026:2007, Hygrothermal Performance of Building Components and Building Elements - Assessment of Moisture Transfer by Numerical simulation;91.100.60, European Committee for Standardization, Brussels, Belgium, 2007.
[79] R. Perez, P. Ineichen, E. Maxwell, R.D. Seals, A. Zelenka, Dynamic global-to-direct irradiance conversion models, Build. Eng. 98 (1) (1992) 354–369.
[80] D. Yang, C.A. Gueymard, Ensemble model output statistics for the separation of direct and diffuse components from 1-min global irradiance, Sol. Energy 208 (2020) 591–603, https://doi.org/10.1016/j.solener.2020.05.082.
[81] M. Rahiminejad, D. Khovalyg, Review on ventilation rates in the ventilated air-spaces behind common wall assemblies with external cladding, Build. Environ. 190 (2021), 107538, https://doi.org/10.1016/j.buildenv.2020.107538.
[82] F. Tariku, E. Iffa, Empirical model for cavity ventilation and hygrothermal performance assessment of wood frame wall systems: experimental study, Build. Environ. 157 (2019) 112–126, https://doi.org/10.1016/j.buildenv.2019.04.020.
[83] J. Langmans, S. Roels, Experimental analysis of cavity ventilation behind rainscreen cladding systems: a comparison of four measuring techniques, Build. Environ. 87 (2015) 177–192, https://doi.org/10.1016/j.buildenv.2015.01.030.
[84] J. Langmans, T.Z. Desta, L. Alderweireldt, S. Roels, Field study on the air change rate behind residential rainscreen cladding systems: a parameter analysis, Build. Environ. 95 (2016) 1–12, https://doi.org/10.1016/j.buildenv.2015.09.012.
[85] J. Falk, K. Sandin, Ventilated rainscreen cladding: measurements of cavity air velocities, estimation of air change rates and evaluation of driving forces, Build. Environ. 59 (2013) 164–176, https://doi.org/10.1016/j.buildenv.2012.08.017.
[86] G.M. Girma, F. Tariku, Experimental investigation of cavity air gap depth for enhanced thermal performance of ventilated rain-screen walls, Build. Environ. 194 (2021), 107710, https://doi.org/10.1016/j.buildenv.2021.107710.
[87] V. Kukk, L. Kaljula, J. Kers, T. Kalamees, Designing highly insulated cross-laminated timber external walls in terms of hygrothermal performance: field measurements and simulations, Build. Environ. 212 (2022), 108805, https://doi.org/10.1016/j.buildenv.2022.108805.
[88] J. Falk, M. Molnár, O. Larsson, Investigation of a simple approach to predict rainscreen wall ventilation rates for hygrothermal simulation purposes, Build. Environ. 73 (2014) 88–96, https://doi.org/10.1016/j.buildenv.2013.11.025.